Optical Functional Units in Zero-Dimensional Metal Halides as a Paradigm of Tunable Photoluminescence and Multicomponent Chromophores

Mingze Li, Maxim S. Molokeev, Jing Zhao, and Zhiguo Xia*

Zero-dimensional (0D) organic–inorganic hybrid luminescent metal halides have many promising optoelectronic applications; however, the single building unit in the 0D framework restricts their multimode optical control and photoluminescence tuning. Thus, it remains urgent but challenging to rationally design distinct anionic polyhedral with different optical functions and further expand this family by an equivalent cation substitution and halogen replacement. Herein, $(C_9NH_{20})_9[Pb_3X_{11}](MX_4)_2$ (X = Br and Cl, M = Mn, Fe, Co, Ni, Cu, and Zn) is successfully synthesized verifying the rationality of the design philosophy, and the optical characterizations demonstrate the effects of X-position anions and M-position cations on luminescence process. Intriguingly, both $[Pb_3X_{11}]^{5-}$ and $[MX_4]^{2-}$ perform as inorganic building units in this 0D system and optically active centers, in which the former leads to high-efficiency broad-band yellow/green emission originating from self-trapped excitons and the as-observed multicomponent chromophores are derived from the absorption of the latter in the visible light region. The present work highlights the importance of different optical functional units showing synergistic effects on the physical properties and inspires future studies to explore multifunctional application of 0D luminescent metal halides.

1. Introduction

Rational structural design of organic–inorganic hybrid metal halides (OIHMH) increasingly attracts attentions due to their unprecedented structural tunability and excellent optoelectronic properties.[1] For instance, two-dimensional (2D) layered OIHMH can be flexibly designed according to their stacking direction—(100)-oriented OIHMH, (110)-

oriented OIHMH, and (111)-oriented OIHMH)—and the numbers of octahedral layers.[2] As a new star material in the OIHMH family, zero-dimensional (0D) OIHMH has received enough interests by their unique 0D structures; however, the structural design of 0D materials is still staying early stage.[3] Selecting appropriate organic ligands and single inorganic building units to form an 0D structure performs as the general principle. However, such a simple design principle quickly encountered its challenge including the limitation of suitable inorganic elements and the monotony of their optical properties. To achieve breakthroughs in material design of 0D OIHMH, several recent studies have been devoted to find mixed 0D systems with two different building units and achieved some exciting achievements.[4] For instance, Han et al. explored a new 0D mixed Bi–Sb OIHMH with ultra-broadband emission,[4a] and Ma discovered a Pb–Zn-based 0D material with near-unity photoluminescence quantum yield (PLQY).[4b] Our group also reported a Pb–Mn based 0D compound with tunable emission depending on temperature and excitation wavelength.[4c] Despite this, the rational design principles for this type of materials are still vague, and the published work appears not to broaden the scope of applications. Thus, designing multiple building units mixed in one lattice and further expanding the application field is undoubtedly the next step in the development of new 0D OIHMH systems.

M. Li, Prof. J. Zhao, Prof. Z. Xia
The Beijing Municipal Key Laboratory of New Energy
Materials and Technologies
School of Materials Sciences and Engineering
University of Science and Technology Beijing
Beijing 100083, P. R. China
E-mail: xiazg@ustb.edu.cn, xiazg@scut.edu.cn
Prof. M. S. Molokeev
Laboratory of Crystal Physics
Kirensky Institute of Physics
Federal Research Center KSC SB RAS
Krasnoyarsk 660036, Russia

Prof. M. S. Molokeev
Siberian Federal University
Krasnoyarsk 660041, Russia
Prof. M. S. Molokeev
Department of Physics
Far Eastern State Transport University
Khabarovsk 680021, Russia
Prof. Z. Xia
State Key Laboratory of Luminescent Materials and Devices and Institute of Optical Communication Materials
South China University of Technology
Guangzhou 510641, China

In general, $[PbX_6]^{2-}$, $[SnX_6]^{2-}$, and $[SbX_5]^{2-}$ (X = Cl, Br) are selected as the inorganic parts of 0D OIHMH to exhibit broadband emission originating from the so-called self-trapped excitons (STEs).[3b,5] Owing to the relatively large band gap, most of the above materials possess transparent body colors which facilitates their photoluminescence in the visible light region. In contrary, metal halides with building units composed by transitional metal ions (Cr^{3+}, Mn^{2+}, Fe^{2+}, Co^{2+}, Ni^{2+}, Cu^{2+}, etc.) appear in various body colors in the visible light region due to their unique electronic transition characteristics.[6] However, these multicomponent chromophores and the stable electronic structures make them difficult to form STEs emission as normally observed in other 0D systems. It is anticipated that combining the above two functional units into a single 0D structural framework may create multifunctional materials.

In this work, we propose a widely applicable design principle of 0D OIHMH that allows two distinct building units with dual-functional properties into a single 0D system, and equivalent cation substitution together with halogen replacement are used to expand this family. Thus, a series of isomorphic 0D materials $(C_9NH_{20})_9[Pb_3X_{11}](MX_4)_2$ ($C_9NH_{20}^+$ = 1-buty-1-methylpyrrolidinium⁺, X = Br, Cl; M = Mn, Fe, Co, Ni, Cu, Zn) with two distinct building units, $[Pb_3X_{11}]^{5-}$ and $[MX_4]^{2-}$, are synthesized as a showcase. We select $[Pb_3X_{11}]^{5-}$ as the fixed component, and typical STEs emission is observed owing to the strong electron–phonon coupling. Simultaneously, $[MX_4]^{2-}$ units with unique absorption characteristics are elected as variable part, therefore, diverse body colors covering almost the entire visible light region appeared. Multiple optical properties derived from different building units make these materials ideal for multifunctional chromophores. Moreover, detailed characterization and analysis of optical properties revealed the different roles of M-position cations and X-position anions. The newly proposed design principle of multifunctional 0D OIHMH with two different optical functional units undoubtedly creates more optical materials with unprecedented multifunctionality.

2. Results and Discussion

The simplified schematic diagram (**Figure 1**a–c) demonstrates the design principle of $(C_9NH_{20})_9[Pb_3X_{11}](MX_4)_2$ (X = Br, Cl; M = Mn, Fe, Co, Ni, Cu, Zn). All of the crystals were prepared by a simple and low-cost solution method, and the synthesis details are shown in Section 4. As a constant part, $[Pb_3Br_{11}]^{5-}$ clusters as an example consist of three symmetric equivalent $[PbBr_6]^{4-}$ octahedra (Figure 1a). As a variable part, $[MX_4]^{2-}$ can be varied depending on the M-position cations (Figure 1b). The asymmetric part of the $(C_9NH_{20})_9[Pb_3X_{11}](MX_4)_2$ (X = Br, Cl; M = Mn, Fe, Co, Ni, Cu, Zn) unit cell is shown in Figure S1, Supporting Information, from which one can clearly observe the coordination of Pb–Br polyhedra. The crystal structure of $(C_9NH_{20})_9[Pb_3X_{11}](MX_4)_2$ were finally determined by the corresponding single crystal X-ray diffraction (SCXRD) data, which all belong to trigonal system and $P31c$ space group. Detailed crystal data and structure refinement were shown in Table S1, Supporting Information and one can also find the crystallographic information files (CIFs) of the studied compounds $(C_9NH_{20})_9[Pb_3Br_{11}](MBr_4)_2$ (M = Mn, Fe, Co, Ni, Zn) and $(C_9NH_{20})_9[Pb_3Cl_{11}]$
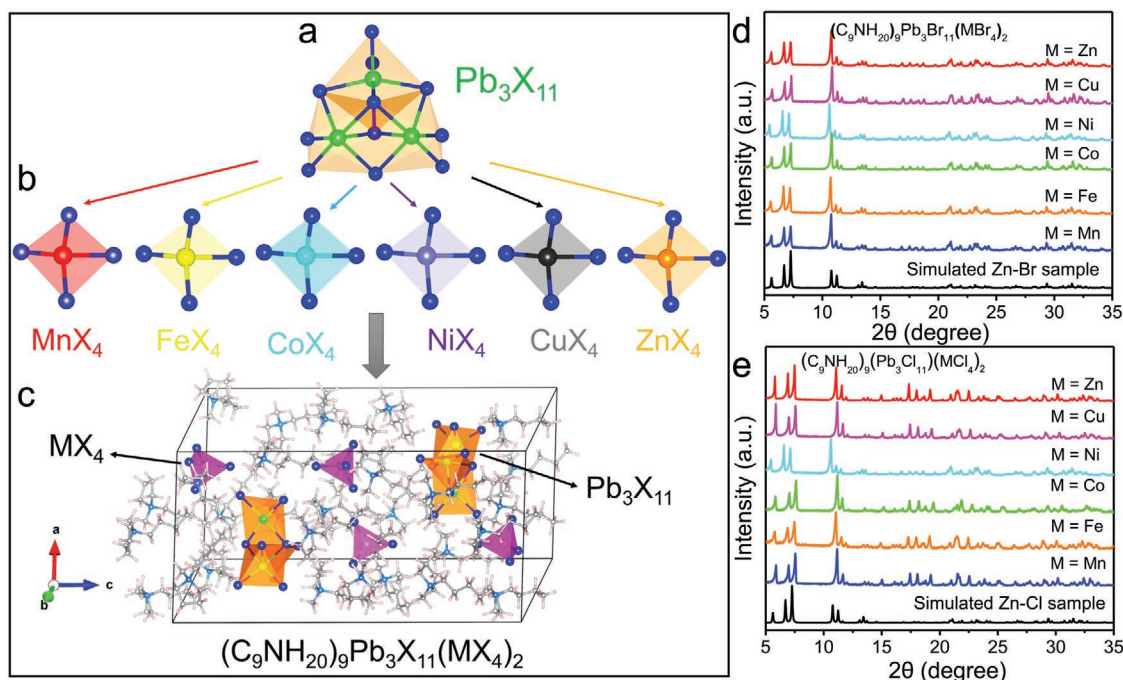
Figure 1. The proposed structural design principle of $(C_9NH_{20})_9[Pb_3X_{11}](MX_4)_2$ (X = Br, Cl; M = Mn, Fe, Co, Ni, Cu, Zn) highlighting the local structure of $[Pb_3X_{11}]^{5-}$ block (a), $[MX_4]^{2-}$ block with different M-position cations (b), and the unit cell of $(C_9NH_{20})_9[Pb_3X_{11}](MX_4)_2$ (c). d) The simulated and experimental X-ray powder patterns of $(C_9NH_{20})_9[Pb_3Br_{11}](MBr_4)_2$ (M = Mn, Fe, Co, Ni, Cu, Zn). e) The simulated and experimental X-ray powder patterns of $(C_9NH_{20})_9[Pb_3Cl_{11}](MCl_4)_2$ (M = Mn, Fe, Co, Ni, Cu, Zn).

**ADVANCED
SCIENCE NEWS**

www.advancedsciencenews.com

**ADVANCED
OPTICAL
MATERIALS**

www.advopticalmat.de
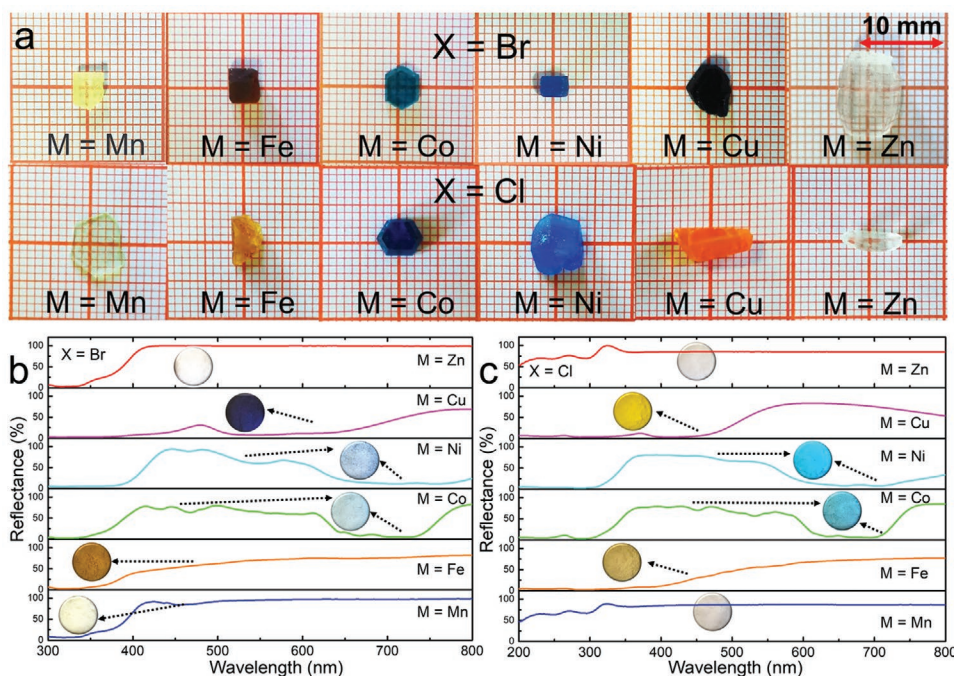
Figure 2. a) Optical photographs of as-grown $(C_9NH_{20})_9[Pb_3X_{11}](MX_4)_2$ (X = Br, Cl; M = Mn, Fe, Co, Ni, Cu, Zn) crystals in the daylight. b,c) UV–vis diffuse reflectance spectra of $(C_9NH_{20})_9[Pb_3X_{11}](MX_4)_2$ powder samples. Inset: optical photographs of powder samples under day light.

$(MCl_4)_2$ (M = Mn, Co, Zn) in the Supporting Information. In addition, simulated and experimental powder X-ray diffraction (PXRD) patterns of $(C_9NH_{20})_9[Pb_3X_{11}](MX_4)_2$ are shown in Figure 1d,e to confirm the purity and isomorphism of all the studied metal halide crystals. We have also used Rietveld refinement to confirm the crystal structure. All peaks were indexed by trigonal cell (P31c) with parameters close to single crystal data (Figure S2 and Table S2, Supporting Information). Profile fitting was performed using TOPAS 4.2. Refinements were stable and gave low R-factors. The refined results undoubtedly confirmed the correctness of our structure and verified the purity of all structures. Due to the ultra-complex structure of this type of compounds, solving their structures is a very difficult work. Nevertheless, in the current work, we have successfully solved eight structures (Mn–Br, Fe–Br, Co–Br, Ni–Br, Zn–Br, Mn–Cl, Co–Cl, and Zn–Cl samples) using SCXRD and verified the isomorphism and purity of other four compounds (Cu–Br, Fe–Cl, Ni–Cl, and Cu–Cl samples). Moreover, thermogravimetric analysis (TGA) data provided in Figure S3, Supporting Information demonstrate their high thermal stability.

Figure 2a shows optical photographs of $(C_9NH_{20})_9[Pb_3X_{11}]$ $(MX_4)_2$ (X = Br, Cl; M = Mn, Fe, Co, Ni, Cu, Zn) crystals under daylight. One can find that all the as-grown crystals possess large size and high transparency suggesting the ultra-high crystal quality in our work. Besides, another interesting phenomenon was the variable body colors of different crystals, which suggest that this type of materials may find potential applications in multifunctional pigments.[7] To further understand such an unusual phenomenon, the UV–vis reflectance spectra of $(C_9NH_{20})_9[Pb_3X_{11}](MX_4)_2$ samples are provided in Figure 2b and Figure 2c, respectively. As the M-position cation and X-position anion change as the color tunable chromophores, the clear

diversity of the absorption in visible region is observed, which leads to the distinct body colors. Such variable absorption characteristics depending on different transition metal halides are undoubtedly attributed to the different charge transfer transition, in which the X-position anions change the outermost p orbitals of halogens while the M-position cations will alter the 3d orbitals of the transition metals. The shift of the absorption peaks with the variable M position cations is consistent with the change of the lowest energy level binding energy caused by the 3d configuration of the monovalent metal ion, and the absorption peaks in our work is similar with previous literature on transitional metal halides.[6a,c] In this work, we successfully obtained crystals with different body colors of purple, blue, cyan, green, yellow, dark yellow, orange, deep red, and colorless that contain almost full-region of the visible light, which provide them large potentiality for using in pigment materials.

Figure 3 comparatively demonstrates the photoluminescent properties of the as-grown $(C_9NH_{20})_9[Pb_3Br_{11}](MBr_4)_2$ (M = Mn, Fe, Co, Ni, and Zn) and $(C_9NH_{20})_9[Pb_3Cl_{11}](MCl_4)_2$ (M = Mn, Fe Co, Ni, Cu, and Zn) crystals, including photoluminescence excitation (PLE) spectra, photoluminescence emission (PL) spectra, and photoluminescence decay curves at room temperature (RT). We illustrate all the samples except $(C_9NH_{20})_9[Pb_3Br_{11}](CuBr_4)_2$ since it does not show photoluminescence in the visible light region. As shown in Figure 3a,c, samples with the same X-position anion exhibit similar photoluminescence properties. Specifically, Br-based samples show broad-band yellow emission peaked at around 565 nm upon the excitation of 365 nm, while Cl-based samples can be efficiently excited at 330 nm and show relatively narrower green emission peaking at around 516 nm. The transformation of the M-position cations hardly affect the emission peak, which make it easy for
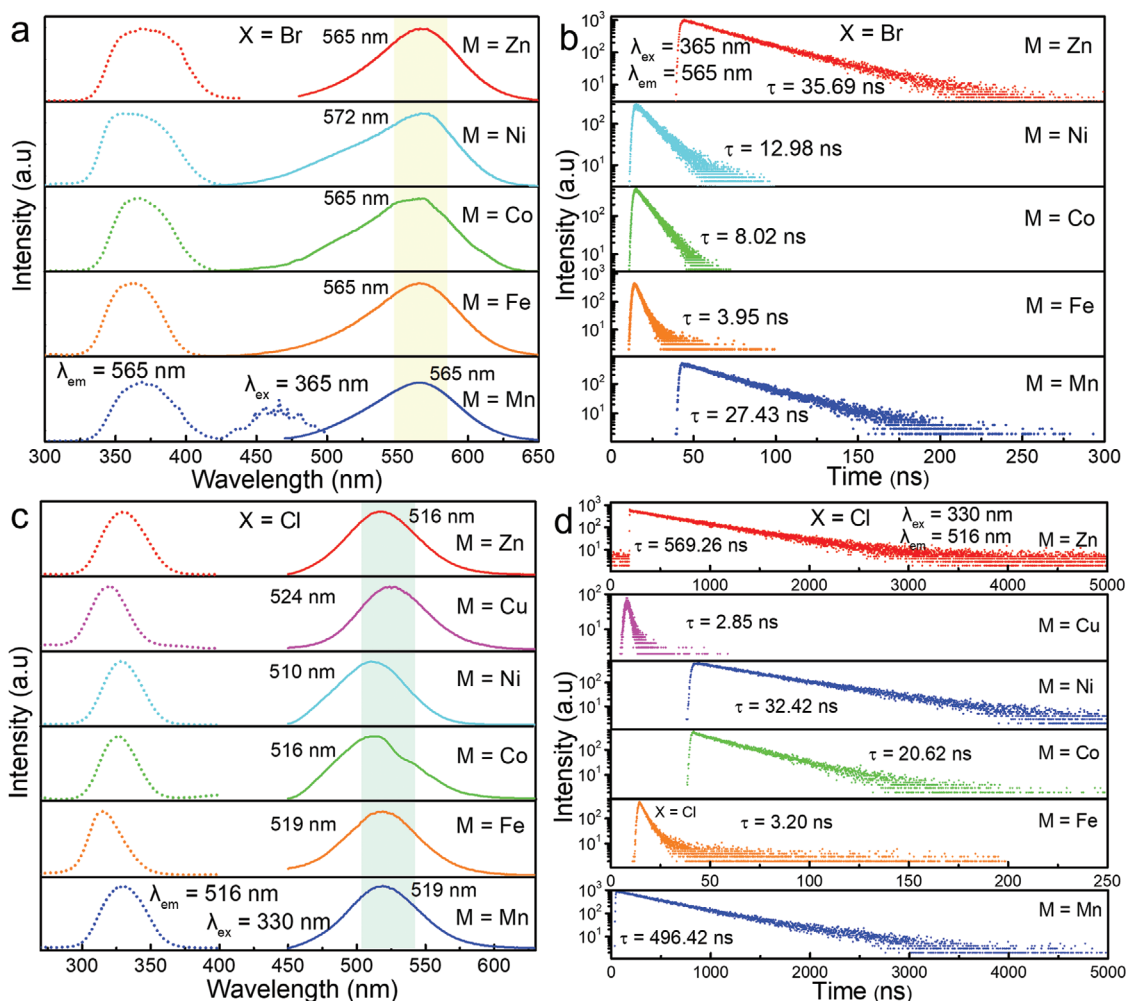
**ADVANCED
SCIENCE NEWS**

www.advancedsciencenews.com

**ADVANCED
OPTICAL
MATERIALS**

www.advopticalmat.de

Figure 3. a) PLE and PL spectra of $(C_9NH_{20})_9[Pb_3Br_{11}](MBr_4)_2$ (M = Mn, Fe, Co, Ni, Zn) at room temperature. b) The room temperature photoluminescence decay curves of $(C_9NH_{20})_9[Pb_3Br_{11}](MBr_4)_2$ crystals monitored the emission at 565 nm upon excitation of 365 nm. c) PLE and PL spectra of $(C_9NH_{20})_9[Pb_3Cl_{11}](MCl_4)_2$ (M = Mn, Fe Co, Ni, Cu, Zn) at room temperature. d) The room temperature photoluminescence decay curves of $(C_9NH_{20})_9[Pb_3Cl_{11}](MCl_4)_2$ crystals monitored the emission at 516 nm upon excitation of 330 nm.

us to attribute the emission center to the $[Pb_3X_{11}]^{5-}$ clusters. Many recent studies show that organic cations may also contribute to the emission in hybrid metal halides; with the aim of determining the role of organic cations in the PL process, we also provided the PL comparison between the organic salt and selected samples (Figure S4, Supporting Information).[8] As shown in the results, the two organic salts exhibit negligible emission compared to the title compounds (about 50 times lower than Zn–Br sample and 300 times lower than Zn–Cl sample). Moreover, the weak blue emission of organic salt is also quite different from the title compounds, so we can conclude that the organic cations show no contribution in this system. Moreover, Figure 3b,d show the decay curves of $(C_9NH_{20})_9[Pb_3Br_{11}]$ $(MBr_4)_2$ and $(C_9NH_{20})_9[Pb_3Cl_{11}](MCl_4)_2$, respectively, and the nanosecond lifetime is consistent with other Pb-based hybrid halides.[9] The above optical parameters demonstrate that the emission of $(C_9NH_{20})_9[Pb_3X_{11}](MX_4)_2$ is derived from the contribution of $[Pb_3X_{11}]^{5-}$ part, and the typical STEs mechanism can be well-explained for the broadband emission (full width at half

maximum (FWHM) ≈75 nm for Br-based samples and ≈61 nm for Cl-based samples) and large Stokes shift (≈200 nm for Br samples and ≈186 nm for Cl samples).[10] It must be pointed out that there is a special compound among the following materials, $(C_9NH_{20})_9[Pb_3Br_{11}](MnBr_4)_2$, which has an extra emission band under 450 nm excitation and thus forms multiple-emission. The PLE and PL spectra of $(C_9NH_{20})_9[Pb_3Br_{11}](MnBr_4)_2$ with excitation wavelength of 450 nm and emission wavelength of 528 nm is provided in Figure S5, Supporting Information. The green emission peaked at 528 nm with the FWHM of 67 nm is undoubtedly attributed to the $^4T_1$–$^6A_1$ transition of Mn^{2+} ions, and the long millisecond lifetime (Figure S6, Supporting Information) further confirms this hypothesis.[11] Such multiple-emission mechanism also provides a promising multi-functional application prospect in white-light emitting devices (WLEDs), which enables 0D materials to be used both in UV-pumped and blue-light-pumped WLEDs. More detailed photo-physical analysis together with the application explorations of $(C_9NH_{20})_9[Pb_3Br_{11}](MnBr_4)_2$ can be found in our recent work.[4c]
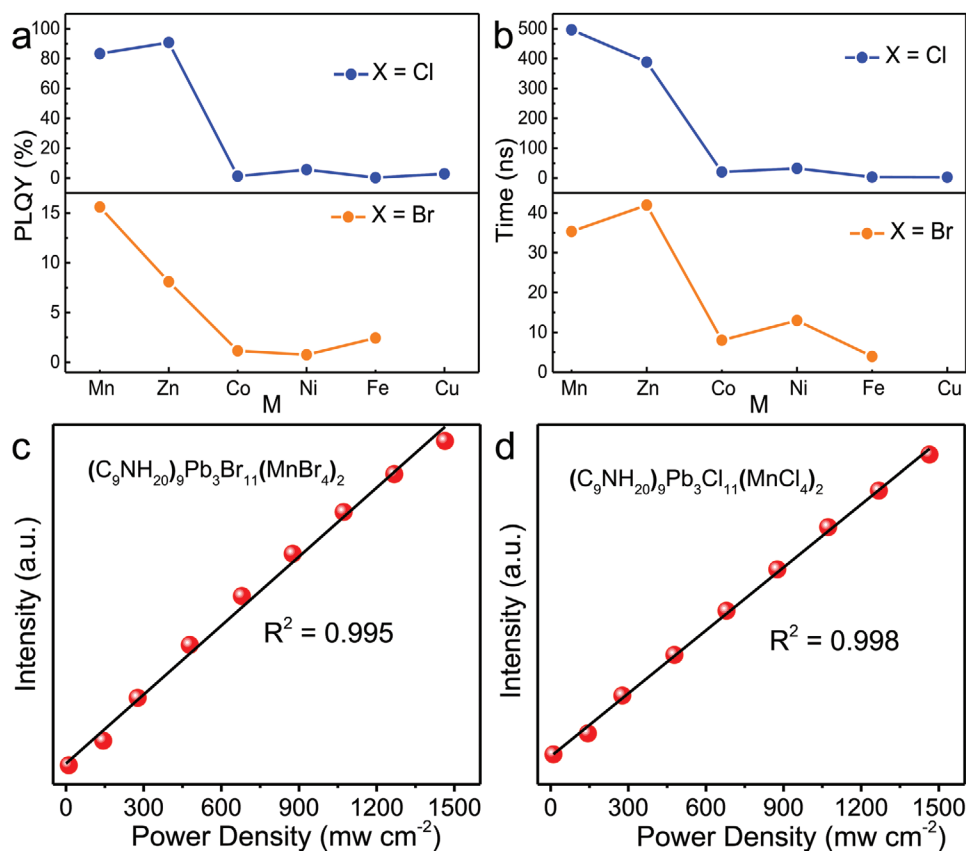
**ADVANCED
SCIENCE NEWS**
www.advancedsciencenews.com

**ADVANCED
OPTICAL
MATERIALS**
www.advopticalmat.de

Figure 4. a) Variations of the PLQY of $(C_9NH_{20})_9[Pb_3Br_{11}](MBr_4)_2$ (M = Mn, Fe, Co, Ni, Zn) and $(C_9NH_{20})_9[Pb_3Cl_{11}](MCl_4)_2$ (M = Mn, Fe Co, Ni, Cu, Zn) with different M-position cations. b) Variations of the photoluminescence decay time of $(C_9NH_{20})_9[Pb_3X_{11}](MX_4)_2$ with different M-position cations. c,d) The emission intensities at 565 nm excited at 375 nm as a function of the excitation power density of the selected sample of $(C_9NH_{20})_9Pb_3Br_{11}(MnBr_4)_2$ and $(C_9NH_{20})_9Pb_3Cl_{11}(MnCl_4)_2$, respectively.

Although the above spectral analysis determines that the $[Pb_3X_{11}]^{5-}$ clusters are mainly responsible for the broadband yellow/green emission; however, there are still two issues that should be explained: (1) How does the different X-position anions affect the luminescence?; (2) In the situation of the same X-position anions, does different M-position cations also have an influence on the emission? Therefore, a careful comparison of the photophysical properties of all samples is necessary. Firstly, the PLE/PL peak of the Cl-based samples have a significant blue shift compared to the Br-based samples, which can be attributed to the excited states with higher energy of Cl-based halides.[12] In addition, as shown in **Figure 4**a,b, Cl-based samples possess higher PLQY (MnCl sample and ZnCl sample even reached high PLQY of 83.3% and 90.8%, respectively, and the original spectra of the two compounds are provided in Figure S7, Supporting Information) and longer photoluminescence decay time, which is probably corresponding to the different emission quenching temperatures defined by the energy barrier for the non-radiative decay.[5a,13] As for the possible effect of M-position cations, we also compared the PLQY (Figure 4a) and photoluminescence decay time (Figure 4b) with the variation of M cations. Interestingly, the results show significant disparity though the samples possess similar PLE/PL spectra, in which Mn-based samples and Zn-based samples have much higher PLQY and longer photoluminescence decay

time compared with other samples. The results can be reasonably explained by combining with previous diffuse reflectance data: Mn-based and Zn-based samples have almost no absorption in the visible light region, in that case the fluorescence will not be affected by the absorption of the material itself; in contrary, other samples all possess relatively stronger absorption in the emission region (450–650 nm), so the self-absorption can partially quench the emission through a fast pathway of de-trapping from STEs to the d level of M^{2+} cation. In this case, Fe-, Co-, Ni-, Cu-based samples possess relatively low PLQY and short life time. One of the most extreme examples of self-absorption is $(C_9NH_{20})_9[Pb_3Br_{11}](CuBr_4)_2$, which absorbs almost all the visible light from 450 to 700 nm and therefore exhibit invisible emission.

Excitation power dependent PL spectra of the selected samples (Figure S8, Supporting Information) were measured and used to exclude the effect of permanent defects which may also cause the fluorescent emissions in 0D OIHMH.[14] As shown in Figure 4c,d, linear relationship between emission intensity and excitation power confirm that the broad-band yellow/green emission is not originated from permanent defects.[15] In order to find direct signal of STEs, a home-made femtosecond pump-probe device was used to measure fs-transient absorption (fs-TA) spectrum.[16] As shown in Figure S9, Supporting Information, the typical absorption characteristic of STEs was found
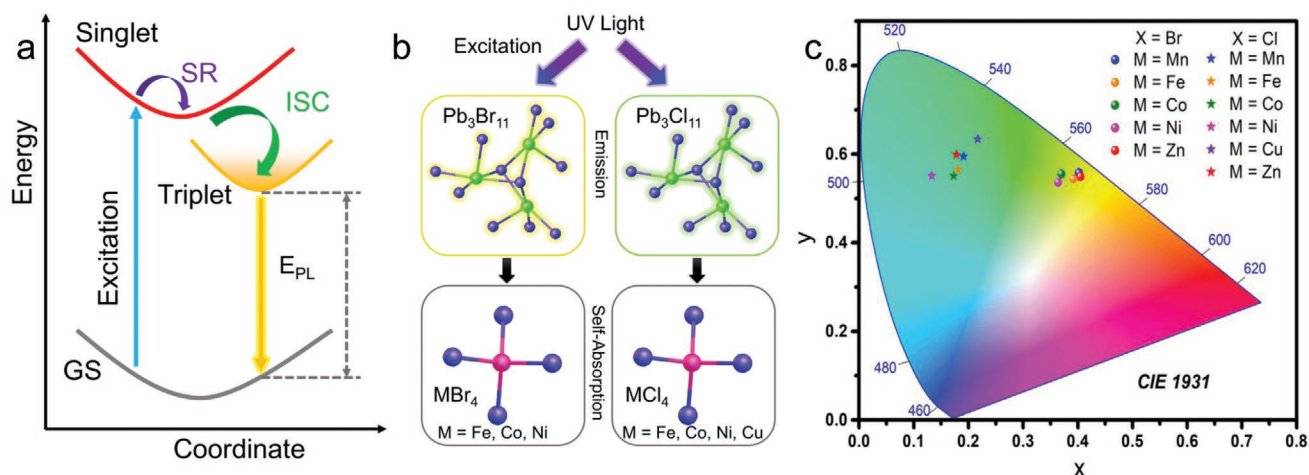
ADVANCED
SCIENCE NEWS
www.advancedsciencenews.com

ADVANCED
OPTICAL
MATERIALS
www.advopticalmat.de

Figure 5. a) Schematic diagram of luminescence processes originating from $[Pb_3X_{11}]$ part; GS, ground state; SR, structural reorganization; ISC, intersystem crossing; E_{PL}, emission energy. b) Proposed models and differences suggesting the photoluminescence and self-absorption of $(C_9NH_{20})_9[Pb_3X_{11}](MX_4)_2$ (X = Br, Cl; M = Mn, Fe, Co, Ni, Cu, Zn). c) CIE chromaticity diagram of $(C_9NH_{20})_9[Pb_3X_{11}](MX_4)_2$ crystals.

which is obvious different with the bleaching signal of permanent defects, and the normalized TA onsets probed at different wavelengths demonstrate the ultra-fast formation time (≈ 200 fs) of STEs (Figure S10, Supporting Information). **Figure 5**a illustrates the luminescence processes of $(C_9NH_{20})_9[Pb_3X_{11}](MX_4)_2$ (X = Br and Cl, M = Mn, Fe, Co, Ni, Cu, and Zn). Under excitations, the electrons of $[Pb_3X_{11}]^{5-}$ part will be excited to the singlet state, and the excited structure (ES) will reorganize in an ultra-fast time and the excitons will transfer to triplet state through intersystem crossing (ISC) process. The efficient radiative combination from triplet state to ground state (GS) bring about the broad-band triplet excitonic emission (also called as STEs emission). The different ES of $[Pb_3Br_{11}]^{5-}$ and $[Pb_3Cl_{11}]^{5-}$ caused by the influence of halogens result in the distinct STEs and eventually showed the difference in the E_{PL}. Figure 5b shows the draft of the role of each two building parts in the luminescence processes, in which $[Pb_3X_{11}]$ unit act as the main character that produces yellow/green fluorescence while $[MX_4]^{2-}$ (M = Co, Ni, Fe, Cu) unit can partly or fully quench the luminescence due to

their strong self-absorption. As a special case of Mn–Br sample, the $[MnBr_4]^{2-}$ unit can also act as an additional emission center while other $[MnX_4]^{2-}$ unit is silent. Although we have not been completely successful in designing multiple active PL functional units in a single 0D frame, we believe that our study provides a feasible solution for this issue. Accordingly, the CIE diagram marked all title compounds as shown in Figure 5c to finely distinguish their luminescent colors. The specific CIE value along with the main optical parameters are listed in **Table 1**, all of which are consistent with our proposed model. The above optical properties with high PLQY and broad-band emission characteristics indicate that this type of materials is promising to be applied in WLEDs as a yellow/green component. Since the thermal stability of emission is one of the important properties for further WLEDs applications, we have measured temperature-dependent PL spectra of Zn–Cl sample. As shown in Figure S11, Supporting Information, the sample can hold about 73% PL intensity at 375 K compared with 300 K. We have also fabricated WLEDs by combining blue commercial

Table 1. Summary of luminescence properties parameters of $(C_9NH_{20})_9[Pb_3Br_{11}](MBr_4)_2$ (M = Mn, Fe, Co, Ni, Zn) and $(C_9NH_{20})_9[Pb_3Cl_{11}](MCl_4)_2$ (M = Mn, Fe Co, Ni, Cu, Zn) with excitation wavelength of 365 nm.

Compound	Peak [nm]	Stokes shift [nm]	FWHM [nm]	PLQY [%]	Lifetime [ns]	CIE (x, y)
$(C_9NH_{20})_9[Pb_3Br_{11}](MnBr_4)_2$	565	200	75	15.6	27.43	(0.402, 0.558)
$(C_9NH_{20})_9[Pb_3Br_{11}](FeBr_4)_2$	565	200	76	2.44	3.95	(0.392, 0.544)
$(C_9NH_{20})_9[Pb_3Br_{11}](CoBr_4)_2$	565	200	81	1.16	8.02	(0.370, 0.555)
$(C_9NH_{20})_9[Pb_3Br_{11}](NiBr_4)_2$	572	207	84	0.76	12.98	(0.364, 0.536)
$(C_9NH_{20})_9[Pb_3Br_{11}](ZnBr_4)_2$	565	200	69	8.1	35.69	(0.405, 0.549)
$(C_9NH_{20})_9[Pb_3Cl_{11}](MnCl_4)_2$	516	186	61	83.3	496.42	(0.191, 0.595)
$(C_9NH_{20})_9[Pb_3Cl_{11}](FeCl_4)_2$	519	205	63	0.31	3.20	(0.181, 0.565)
$(C_9NH_{20})_9[Pb_3Cl_{11}](CoCl_4)_2$	516	190	66	1.32	20.62	(0.173, 0.551)
$(C_9NH_{20})_9[Pb_3Cl_{11}](NiCl_4)_2$	510	182	60	5.71	32.42	(0.133, 0.551)
$(C_9NH_{20})_9[Pb_3Cl_{11}](CuCl_4)_2$	524	204	59	2.89	2.85	(0.217, 0.634)
$(C_9NH_{20})_9[Pb_3Cl_{11}](ZnCl_4)_2$	516	186	61	90.8	569.26	(0.178, 0.599)

**ADVANCED
SCIENCE NEWS**

www.advancedsciencenews.com

**ADVANCED
OPTICAL
MATERIALS**

www.advopticalmat.de

phosphor ($BaMgAl_{10}O_{17}$:Eu^{2+} (BAM:Eu^{2+})), green-emissive $(C_9NH_{20})_9[Pb_3Cl_{11}](ZnCl_4)_2$, the commercial red phosphor $CaAlSiN_3$, and 365 nm near-UV LED chip (Figure S12, Supporting Information). The fabricated WLEDs show ultrahigh color rendering index (CRI, Ra) of 96.3 along with CIE color coordinate of (0.319, 0.372) and the correlated color temperature (CCT) of 5209 K, which all show the future WLEDs applications of this type materials.

3. Conclusion

In summary, by introducing a new design principle for the discovery of new 0D materials with different optical building units, we successfully obtained a series 0D OIHMH $(C_9NH_{20})_9[Pb_3X_{11}](MX_4)_2$ (X = Br, Cl; M = Mn, Fe, Co, Ni, Cu, Zn), featuring two distinct anionic polyhedral named $[Pb_3X_{11}]^{5-}$ and $[MX_4]^{2-}$. The different absorption of $[MX_4]^{2-}$ in the visible light region endows the materials different body colors, while the STEs of $[Pb_3X_{11}]^{5-}$ lead to the yellow/green broad-band emission. The multiple optically active centers enable this type compounds to be used both in photoluminescence materials and pigment materials. By carefully analyzing the spectral data, we summarize the effects of X-position anions and M-position cations on luminescence process and finally propose a reasonable luminescence mechanism. This new type 0D OIHMH with multi-polyhedral structure provides a new direction for the design of new 0D materials and is expected to be applied in the field of other multifunctional materials.

4. Experimental Section

Materials and Preparation: Manganese (II) bromide ($MnBr_2$) (99.9%), nickel (II) bromide (99.9%), cupric (II) bromide (99.95%), zinc (II) bromide (99.9%), manganese (II) chloride ($MnCl_2$) (99.99%), iron (II) chloride (99.5%), cobalt (II) chloride (99.7%), cupric (II) chloride (99.99%), zinc (II) chloride (99.99%), lead bromide (99%), lead chloride (99.99%), 1-buty-1-methylpyrrolidinium bromide ($C_9NH_{20}Br$) (99%), 1-buty-1-methylpyrrolidinium chloride ($C_9NH_{20}Cl$) (99%), and *N*, *N*-dimethylformamide (DMF) (99.9%) were purchased from Aladdin Co. Ltd. (Shanghai, China). Iron (II) bromide (98%), cobalt (II) bromide (97%), and nickel (II) chloride (99%) were purchased from Energy Chemical (Shanghai, China). $(C_9NH_{20})_9[Pb_3X_{11}](MX_4)_2$ (X = Br, Cl; M = Mn, Fe, Co, Ni, Cu, Zn) single crystals were synthesized as follows: 4.5 mmol of $C_9NH_{20}Br$/$C_9NH_{20}Cl$, 1.0 mmol of MX_2, and 1.5 mmol of PbX_2 were dissolved in 1.5 mL of DMF under heating and continuous stirring at 323 K. Yellow crystals were obtained by slowly cooling the saturated solution to room temperature with the controlled cooling rate to obtain the crystals with different sizes. All chemicals were used as received from the vendors without further purification.

Characterization: The diffraction patterns were collected from single crystals of $(C_9NH_{20})_9[Pb_3X_{11}](MX_4)_2$ (X = Br, Cl; M = Mn, Fe, Co, Ni, Cu, Zn) at 296 K using the SMART APEX II X-ray single crystal diffractometers (Bruker AXS, analytical equipment of Krasnoyarsk Center of collective use of SB RAS) equipped with a CCD-detector, graphite monochromator, and Mo Kα radiation source. The absorption corrections were applied using the SADABS program. The structures were solved by the direct methods using package SHELXS and refined using the SHELXL program.[17] All hydrogen atoms were linked with C,N atoms and positioned geometrically as riding on their parent atoms with $U_{iso}(H) = U_{eq}(C,N)$. The DIAMOND program[18] is used for the crystal structure plotting. Powder X-ray diffraction (PXRD) data

of $(C_9NH_{20})_9[Pb_3X_{11}](MX_4)_2$ (X = Br, Cl; M = Mn, Fe, Co, Ni, Cu, Zn) was obtained using diffractometer D8 ADVANCE (Bruker) equipped by a VANTEC detector with an Ni filter. The measurements were made using Cu Kα radiation. The structural parameters defined by single crystal analysis were used as a basic in powder pattern Rietveld refinement. The refinement was produced using TOPAS 4.2 software.[19] Thermogravimetric analysis (TGA) were performed on a Setaram Labsys Evo at 10 °C min⁻¹ in an argon flow from room temperature to 800 °C. The diffuse reflection spectra were measured on a UV–vis–NIR spectrophotometer (SHIMADZU UV-3600) supplied with an integrating sphere. The photoluminescence excitation (PLE) and emission (PL) spectra at room temperature were recorded by an Edinburgh FLS920 fluorescence spectrophotometer with the Xe900 lamp as the excitation source. The PLQY of Mn–Br, Fe–Br, Co–Br, Ni–Br, Zn–Br, Fe–Cl, Co–Cl, Ni–Cl, and Cu–Cl samples were measured using the integrated sphere on the same FLS920 instrument, and white $BaSO_4$ powder was used as a reference to measure the absorption. The PLQY of Mn–Cl and Zn–Cl samples were measured using Hamamatsu absolute PL quantum yield spectrometer C11347 Quantaurus_QY. The luminescence decay curves were obtained by the FLS920 using an nF900 and µF900 flash lamp and as the excitation source. The power-dependent photoluminescence spectra were measured using the 375 nm (LE-LS-375-140TFCA, 1–140 mW) laser. The PL spectra, color-rendering index (R_a), and correlated color temperature (CCT) of the as-fabricated WLEDs were collected by an integrating sphere spectroradiometer system (ATA-1000, Everfine).

Supporting Information

Supporting Information is available from the Wiley Online Library or from the author.

Conflict of Interest

The authors declare no conflict of interest.

[1] a) Z. Song, J. Zhao, Q. Liu, *Inorg. Chem. Front.* **2019**, *6*, 2969; b) D. B. Mitzi, *J. Chem. Soc., Dalton Trans.* **2001**, *1*, 1; c) B. Saparov, D. B. Mitzi, *Chem. Rev.* **2016**, *116*, 4558; d) Y. Zhao, K. Zhu, *Chem. Soc. Rev.* **2016**, *45*, 655; e) K. Chen, L. Li, *Adv. Mater.* **2019**, *31*, 1901115.

[2] a) L. Mao, W. Ke, L. Pedesseau, Y. Wu, C. Katan, J. Even, M. R. Wasielewski, C. C. Stoumpos, M. G. Kanatzidis, *J. Am. Chem. Soc.* **2018**, *140*, 3775; b) M. D. Smith, A. Jaffe, E. R. Dohner, A. M. Lindenberg, H. I. Karunadasa, *Chem. Sci.* **2017**, *8*, 4497.

ADVANCED
SCIENCE NEWS
www.advancedsciencenews.com

ADVANCED
OPTICAL
MATERIALS
www.advopticalmat.de

[3] a) H. Lin, C. Zhou, Y. Tian, T. Siegrist, B. Ma, *ACS Energy Lett.* **2017**, *3*, 54; b) V. Morad, Y. Shynkarenko, S. Yakunin, A. Brumberg, R. D. Schaller, M. V. Kovalenko, *J. Am. Chem. Soc.* **2019**, *141*, 9764.

[4] a) R. Zhang, X. Mao, Y. Yang, S. Yang, W. Zhao, T. Wumaier, D. Wei, W. Deng, K. Han, *Angew. Chem., Int. Ed.* **2019**, *58*, 2725; b) C. Zhou, H. Lin, J. Neu, Y. Zhou, M. Chaaban, S. Lee, M. Worku, B. Chen, R. Clark, W. Cheng, J. Guan, P. Djurovich, D. Zhang, X. Lü, J. Bullock, C. Pak, M. Shatruk, M.-H. Du, T. Siegrist, B. Ma, *ACS Energy Lett.* **2019**, *4*, 1579; c) M. Li, J. Zhou, G. Zhou, M. S. Molokeev, J. Zhao, V. Morad, M. V. Kovalenko, Z. Xia, *Angew. Chem., Int. Ed.* **2019**, *58*, 18670.

[5] a) S. Yakunin, B. M. Benin, Y. Shynkarenko, O. Nazarenko, M. I. Bodnarchuk, D. N. Dirin, C. Hofer, S. Cattaneo, M. V. Kovalenko, *Nat. Mater.* **2019**, *18*, 846; b) C. Zhou, H. Lin, Y. Tian, Z. Yuan, R. Clark, B. Chen, L. J. van de Burgt, J. C. Wang, Y. Zhou, K. Hanson, Q. J. Meisner, J. Neu, T. Besara, T. Siegrist, E. Lambers, P. Djurovich, B. Ma, *Chem. Sci.* **2018**, *9*, 586; c) M. D. Smith, B. L. Watson, R. H. Dauskardt, H. I. Karunadasa, *Chem. Mater.* **2017**, *29*, 7083.

[6] a) Y. Sakisaka, T. Ishii, T. Sagawa, *J. Phys. Soc. Jpn.* **1974**, *36*, 1365; b) C. R. Ronda, H. H. Siekman, C. Haas, *Physica B+C* **1987**, *144*, 331; c) C. Liu, Z. Xia, M. Chen, M. S. Molokeev, Q. Liu, *J. Chem. Phys.* **2001**, *114*, 7388; d) X.-B. Wang, L.-S. Wang, R. Brown, P. Schwerdtfeger, D. Schröder, H. Schwarz, *J. Chem. Phys.* **2001**, *114*, 7388.

[7] C. Liu, Z. Xia, M. Chen, M. S. Molokeev, Q. Liu, *Inorg. Chem.* **2015**, *54*, 1876.

[8] a) A. Yangui, R. Roccanova, T. M. McWhorter, Y. Wu, M.-H. Du, B. Saparov, *Chem. Mater.* **2019**, *31*, 2983; b) A. Yangui, R. Roccanova, Y. Wu, M.-H. Du, B. Saparov, *J. Phys. Chem. C* **2019**, *123*, 22470.

[9] a) L. Mao, P. Guo, M. Kepenekian, I. Hadar, C. Katan, J. Even, R. D. Schaller, C. C. Stoumpos, M. G. Kanatzidis, *J. Am. Chem. Soc.* **2018**, *140*, 13078; b) C. Zhou, H. Lin, M. Worku, J. Neu, Y. Zhou, Y. Tian, S. Lee, P. Djurovich, T. Siegrist, B. Ma, *J. Am. Chem. Soc.* **2018**, *140*, 13181.

[10] S. Li, J. Luo, J. Liu, J. Tang, *J. Phys. Chem. Lett.* **2019**, *10*, 1999.

[11] a) K. E. Lawson, *J. Chem. Phys.* **1967**, *47*, 3627; b) Y. Rodríguez-Lazcano, L. Nataf, F. Rodríguez, *Phys. Rev. B* **2009**, *80*, 085115; c) M. Li, J. Zhou, M. S. Molokeev, X. Jiang, Z. Lin, J. Zhao, Z. Xia, *Inorg. Chem.* **2019**, *58*, 13464.

[12] a) R. Gautier, M. Paris, F. Massuyeau, *J. Am. Chem. Soc.* **2019**, *141*, 12619; b) X. Li, P. Guo, M. Kepenekian, I. Hadar, C. Katan, J. Even, C. C. Stoumpos, R. D. Schaller, M. G. Kanatzidis, *Chem. Mater.* **2019**, *31*, 3582.

[13] a) P. W. M. Jacobs, *J. Phys. Chem. Solids* **1991**, *52*, 35; b) K. M. McCall, C. C. Stoumpos, S. S. Kostina, M. G. Kanatzidis, B. W. Wessels, *Chem. Mater.* **2017**, *29*, 4129.

[14] J. Zhou, M. Li, L. Ning, R. Zhang, M. S. Molokeev, J. Zhao, S. Yang, K. Han, Z. Xia, *J. Phys. Chem. Lett.* **2019**, *10*, 1337.

[15] T. Hu, M. D. Smith, E. R. Dohner, M. J. Sher, X. Wu, M. T. Trinh, A. Fisher, J. Corbett, X. Y. Zhu, H. I. Karunadasa, A. M. Lindenberg, *J. Phys. Chem. Lett.* **2016**, *7*, 2258.

[16] a) S. Q. Yang, Y. Zhang, K. L. Han, *J. Lumin.* **2019**, *206*, 46; b) S. Q. Yang, K. L. Han, *J. Phys. Chem. A* **2016**, *120*, 4961.

[17] G. M. Sheldrick, *Acta Crystallogr. A* **2008**, *64*, 112.

[18] K. Brandenburg, M. Berndt, Postfach 1251, D-53002 Bonn, Germany **2004**.

[19] V. Topas, Bruker AXS, Karlsruhe, Germany **2008**.